Applying gradient tree boosting to QTL mapping with Shapley additive explanations

Tomohiro Ishibashi, Akio Onogi*

Department of Life Sciences, Faculty of Agriculture, Ryukoku University, Otsu, Shiga, 520-2194, Japan

Corresponding author:

Akio Onogi

Postal address: 1-5, Yokotani, Oe-cho, Seta, Otsu, Shiga, 520-2194, Japan

Phone: +81-(0)77-599-5719

E-mail: onogiakio@gmail.com

ORCID: 0000-0003-1707-9539

Running head

Applying XGB-SHAP to QTL mapping

Keywords

Epistasis, gene interaction, variable selection, association mapping, SHAP

Abstract

Mapping quantitative trait loci (QTLs) is one of the major goals of quantitative genetics; however, identifying the interactions between QTLs (i.e., epistasis) remains challenging. Recently developed machine learning methods, such as deep learning and gradient boosting, are transforming the real world. These methods could advance QTL mapping methodologies because of their high capability for capturing complex relationships among features. One problem with applying such complex models to QTL mapping is evaluation of feature importance. In this study, XGBoost, a popular gradient tree boosting algorithm, was applied for QTL mapping in biparental populations with Shapley additive explanations (SHAPs). SHAP is a local (i.e., instance-wise) importance index with the desired properties as feature importance indices. The SHAP-assisted XGBoost (SHAP-XGB) was compared with conventional methods, including composite interval mapping (CIM), multiple interval mapping (MIM), inclusive CIM (ICIM), and BayesC, using simulations and rice heading date data. SHAP-XGB performed comparable to CIM, MIM, ICIM, and BayesC in mapping main QTL effects and was superior to MIM, ICIM, and BayesC in mapping QTL interaction effects. As SHAP can evaluate local importance, interactions between markers can be visualized by plotting SHAP interaction values for each instance (plant/line). These results illustrated the strength of SHAP-XGB in detecting and interpreting epistatic QTLs and suggest the possibility that SHAP-XGB complements conventional methods.

Article summary

Recently developed machine learning methods are transforming the real world. These methods could advance QTL mapping methodologies because of their high capability for capturing complex relationships among features. Here, XGBoost, a popular gradient tree boosting algorithm, was applied for QTL mapping in biparental populations with Shapley additive explanations (SHAPs). This SHAP-assisted XGBoost was shown to be useful for mapping and interpreting QTL interactions and can complement conventional methods, such as multiple interval mapping, inclusive composite interval

mapping, and Bayesian regression.

Introduction

Detecting quantitative trait loci (QTLs) underpinning variations in quantitative traits is one of the major goals in analyzing quantitative traits. Detecting QTLs can lead to useful applications such as efficient selection based on QTL genotypes, genomic engineering to modify phenotypes, development of medical technologies by understanding molecular mechanisms, and advancing quantitative genetics theories by deciphering the genetic architecture of quantitative traits (Falconer and Mackay 1996). Interval mapping (IM) is a typical method to detect QTLs in inbred line crosses (Lander and Botstein 1989). IM tests associations of each marker and marker interval with the phenotypes independently. In practice, composite IM (CIM), an extension of IM, is the most popular method (Jansen and Stam 1994; Zeng 1994). CIM considers markers linked with major QTLs as cofactors to enhance detection power and precision when multiple QTLs exist.

Interactions between QTLs, known as epistasis, have also been of interest in quantitative genetics because genes (proteins) function in corporations. Detecting epistatic QTLs will broaden the applications of the QTLs described above and will be helpful to depict gene networks underlying complex quantitative traits. A successful example of QTL and epistatic QTL mapping in plant breeding is the rice heading date. To date, a number of QTL/genes and their networks under short- and long-day conditions have been elucidated (Hori et al. 2016; Wei et al. 2020). Methods for detecting epistatic QTLs include multiple interval mapping (MIM, Kao et al. 1999; Laurie et al. 2014), inclusive CIM (ICIM, Li et al. 2008), and Bayesian regression where whole genome-wide markers are used as explanatory variables simultaneously (Zhang and Xu 2005; Li and Sillanpää 2012). A method to detect interactions between QTLs and genetic background was also proposed (Jannink and Jansen 2001). Detection of QTL/gene interactions has been of interest in genome-wide association studies (GWAS), although detection is more difficult than in inbred line crosses because of the generally low allele frequencies. These methods include hierarchical Bayesian modeling for high-order gene interactions

(Bayesian high-order interaction toolkit (BHIT) (Wang et al. 2015) and a marginal epistasis test (MAPIT) (Crawford et al. 2017).

Recent machine learning models, such as gradient boosting and deep neural networks, have shown high predictive abilities in various applications. Because these models are inherently capable of capturing complex interactions among features, they are expected to be useful for QTL mapping, particularly for complex QTL interactions. However, unlike linear regressions, the contributions of each feature and feature interaction are not explicitly outputted. Thus, such complex models should be used with efficient and reliable methods to extract the importance of features for selection. For example, Johnsen et al. (2021) applied Shapley additive explanations (SHAP) to estimate the feature importance of extreme gradient boosting (XGBoost) (Chen and Guestrin 2016) in a GWAS using UK Biobank data. Cui et al. (2022) applied a Shapley-based interaction score (Sundararajan et al. 2020) to deep neural networks to identify gene-gene interactions in a GWAS. The Shapley value was originally proposed to evaluate players' contributions to rewards in cooperative games (Shapley 1953). By considering players and rewards as features and prediction outcomes, respectively, the Shapley value can be used to evaluate the feature and feature combination importance of the prediction models. SHAP is based on the Shapley value and is characterized by the local importance of the feature; that is, the importance of the feature for each instance (i.e., sample) is estimated (Lundberg and Lee 2017). Because the summation of the SHAP values of the features for an instance is equal to the predicted values of the instance (a property called local accuracy), it is feasible to determine which features have a large impact on the prediction of the instance (Lundberg and Lee 2017; Lundberg et al. 2018). SHAP also has two additional properties–missingness and consistency–that are desirable as feature importance indices.

It may be possible to map QTLs and QTL interactions using SHAP or Shapley value-based scores and recently advanced machine learning more efficiently and effectively than conventional methods. The GWASs mentioned above partially prove this possibility; however, evaluation studies are limited. Therefore, several issues remain unresolved. For example, the effect of overfitting complex models to

data on the efficiency of QTL mapping remains unclear. Moreover, the translation of SHAP values into signals for QTL detection has not been thoroughly examined. The properties of mapping dominance effects are also underexamined. In addition, comparisons with conventional methods such as CIM, MIM, ICIM, and Bayesian regressions have not been conducted. In this study, we evaluated the potential of XGBoost for QTL and epistatic QTL mapping using SHAP. XGBoost is an algorithm for gradient boosting, which is a class of ensemble learning (Chen and Guestrin 2016). XGBoost was selected because it is one of the most prevalent gradient boosting algorithms. We characterized this SHAP-assisted XGBoost (SHAP-XGB) by applying the method to simulated and real biparental populations and comparing it with conventional methods. The results illustrated the strength of SHAP-XGB in detecting and interpreting epistatic QTLs, as expected, and suggested the possibility that SHAP-XGB complements conventional methods.

Materials and Methods

Extreme gradient boosting

XGBoost is based on decision trees and represents the response of instance *i* (the phenotype of plant/line *i* in the case of QTL mapping), y_i, with the linear combination of *K* decision trees as

$$\hat{y}_i = \sum_{k=1}^{K} f_k(x_i),$$

where f is a tree with structure *q* and leaf weight *w* and x_i is the vector of feature (marker genotypes in the case of QTL mapping). In other words, y_i is represented as the sum of the outputs of multiple decision trees. The decision trees are sequentially added at each iteration. Thus, the objective function of XGBoost at iteration *t*, that is, when adding *t*th tree, can be written as

$$L^t = \sum_{i=1}^{n} l\left(y_i, \quad \hat{y}_i^{t-1} + f_t(x_i)\right) + \Omega(f_t),$$

where *n* is the number of instances (plants/lines), l is a loss function, $\hat{y}_i^{t-1}$ is $\hat{y}_i$ at iteration $t-1$, f_t is the tree added at iteration *t*, and Ω is a penalty function on the tree structure (i.e., the number of leaves and weights). A penalty function is added to avoid overfitting the model. By approximating f

with Taylor expansions and dropping the constant terms, the objective function becomes

$$\tilde{L}^t = \sum_{j=1}^{T}\left[\left(\sum_{i\in I_j} g_i\right) w_j + \frac{1}{2}\left(\sum_{i\in I_j} h_i + \lambda\right) w_j^2\right] + \gamma T,$$

where g_i and h_i are the first and second order gradients of the loss function, I_j is the set of instances assigned to leaf j, T is the number of leaves, and λ and γ are the regularization parameters. The optimal weight of leaf j (w_j^*) and the corresponding optimal value of $\tilde{L}^{t*}$ are

$$w_j^* = -\frac{\sum_{i\in I_j} g_i}{\sum_{i\in I_j} h_i + \lambda} \text{ and } \tilde{L}^{t*} = -\frac{1}{2}\sum_{j=1}^{T}\frac{\left(\sum_{i\in I_j} g_i\right)^2}{\sum_{i\in I_j} h_i + \lambda} + \gamma T,$$

respectively. Using these results, whether a leaf I should be split into I_L and I_R can be evaluated with the following equation:

$$\frac{1}{2}\left[\frac{\left(\sum_{i\in I_L} g_i\right)^2}{\sum_{i\in I_L} h_i + \lambda} + \frac{\left(\sum_{i\in I_R} g_i\right)^2}{\sum_{i\in I_R} h_i + \lambda} - \frac{\left(\sum_{i\in I} g_i\right)^2}{\sum_{i\in I} h_i + \lambda}\right] - \gamma.$$

This equation was derived by subtracting $\tilde{L}^{t*}$ when leaf I was split into I_L and I_R from $\tilde{L}^{t*}$ when leaf I was a single leaf. Thus, when this equation is positive, $\tilde{L}^{t*}$ decreases because of splitting. XGBoost uses this formula to search for the tree structures to be added, making the method fast and scalable. The authors proposed exact greedy and approximate algorithms for this type of search.

Shapley values

In cooperative game theory, the Shapley value measures how much each player contributes to the game's reward. Assessing the contributions of individual players independently is insufficient in cooperative games because there are usually interactions between players. The core concept of Shapley's value is the 'marginal contribution'. Marginal contribution represents the extent to which a player's participation in a cooperative game increases the game's rewards. This varies according to the combination of players and order of participation. Therefore, the Shapley value of a player is defined by calculating the marginal contribution of a player to all possible player combinations and participation orders and taking their average. In other words, the Shapley value is the average marginal contribution of the player. The Shapley value for player i is defined as follows:

$$\varphi_i = \sum_{S \subseteq N \setminus \{i\}} \frac{|S|!(M-|S|-1)!}{M!} [f(S \cup \{i\}) - f(S)] \quad (1),$$

where N is a set of players, S is a subset of players, M is the number of players, and f is the function that outputs rewards for the given players.

SHAP

Players of Shapley values are replaced with features, and rewards are replaced with the model output (e.g., fitter/predicted phenotypes) in SHAP. The model function to output the rewards given to players takes the form of the expected values, that is, $f(S)$ in Eq. (1) is expressed as $E[f(x)|x_S]$ in SHAP, where x and x_S indicate all features and the features in subset S, respectively. Thus, the SHAP value of feature i of an instance is

$$\varphi_i = \sum_{S \subseteq N \setminus \{i\}} \frac{|S|!(M-|S|-1)!}{M!} \left[E\left[f(x)|x_{S \cup \{i\}}\right] - E[f(x)|x_S]\right]. \quad (2)$$

SHAP is an additive feature-contribution method with three properties: local accuracy, missingness, and consistency. Local accuracy indicates that the summation of the feature contributions defined by Eq. (2) and is equal to the output of the model. Missingness means that importance is not assigned to a missing feature. Consistency implies that if the model is changed such that a feature has a greater impact on the model, the contribution assigned to that feature does not decrease.

The interaction index was used to assess the impact of one feature of a model when combined with another. The Shapley interaction index between features i and j is calculated as (Fujimoto et al. 2006),

$$\varphi_{ij} = \sum_{S \subseteq N \setminus \{i,j\}} \frac{|S|!(M-|S|-2)!}{2(M-1)!} \delta_{ij}(S), \quad (3)$$

where $\delta_{ij}(S) = f(S \cup \{i,j\}) - f(S \cup \{i\}) - f(S \cup \{j\}) + f(S)$. The SHAP interaction value was calculated by replacing the function $f(S)$ with expectations, as shown in Eq. (2). The SHAP interaction value is split equally between each feature combination, that is, $\varphi_{ij} = \varphi_{ji}$. Thus, total interaction effects are calculated as $\varphi_{ij} + \varphi_{ij} = 2\varphi_{ij}$. The SHAP value ($\varphi_i$) of feature i for an instance is decomposed to the main effect of the feature (φ_{ii}) and the interaction effects between the feature

and the others as

$$\varphi_i = \varphi_{ii} + \sum_{j \neq i} \varphi_{ij}.$$

That is, the main effect of feature i is obtained by subtracting the SHAP interaction value between feature i and j ($j \neq i$) from the SHAP value of feature i.

Lundberg et al. (2018) proposed an efficient algorithm for calculating SHAP values from tree-based machine learning models (referred to as Tree SHAP). The algorithm exploits the differences in outputs between models with and without a particular feature using a tree structure to evaluate $E[f(x)|x_S]$. The algorithm was implemented in R package xgboost (ver. 1.7.5.1).

Algorithm of SHAP-XGB

The algorithm of SHAP-XGB is described below and illustrated in Figure 1.

Step 1: Create a bootstrap dataset.

Step 2: Fit an XGBoost model to the dataset, with early stopping determined from the remaining samples. The xgboost R package was used in this study.

Step 3: Calculate the SHAP values (φ_i) from the fitted samples.

Step 4: Decompose the SHAP values into the SHAP interaction values (φ_{ij}) and the remaining values (φ_{ii}).

Step 5: Repeat steps 1–4 100 times and calculate the average of φ_i, φ_{ij}, and φ_{ii}. Note that these values are measures of local importance (i.e., for each line).

Step 6: Average the absolute values of the values obtained in Step 5 across lines to obtain global importance. The averages of the absolute values of φ_i or φ_{ii} are referred to as the global SHAP scores and the averages of the absolute values of $2\varphi_{ij}$ are referred to as the global SHAP interaction scores.

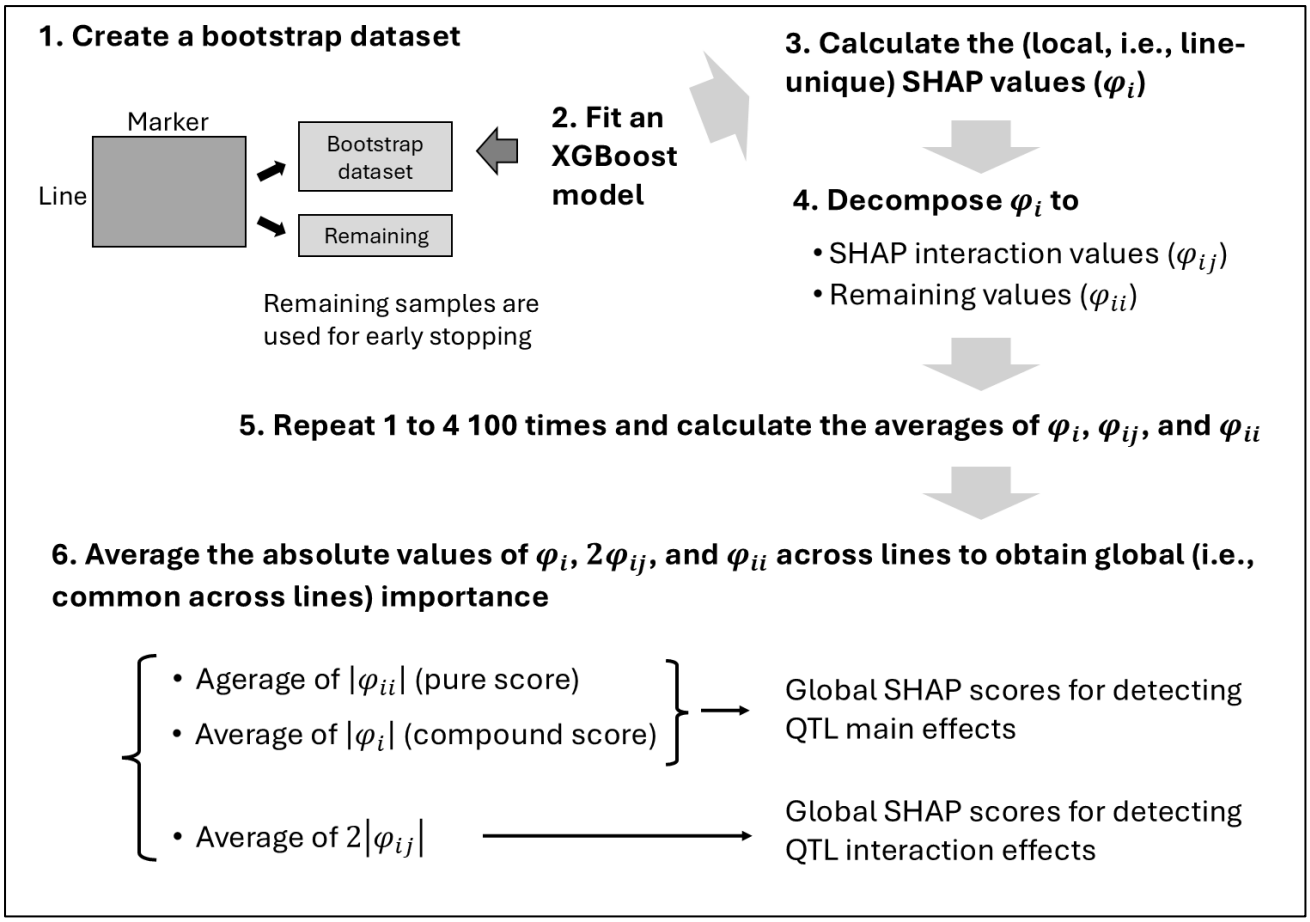

Figure 1 Illustrations of the Shapley additive explanations-assisted XGBoost (SHAP-XGB) algorithm.

Four notifications were added to these algorithms. First, although the absolute SHAP values are averaged across lines to obtain the global importance in Step 6, the consistency property still holds for the global importance scores (Lundberg et al. 2018). Second, bootstrapping was conducted to separate the data into training and validation sets, which were used for early stopping to prevent overfitting. Therefore, other resampling methods could be applied. The number of bootstrap replicates (100) was determined arbitrarily. Thus, fewer numbers—even one—may be acceptable, albeit with a loss of reliability of the SHAP values. Third, default values were used for the hyperparameters of xgboost except for the "early_stopping_rounds" argument, which was set to three. This argument specifies the number of rounds in which the boosting iterations stop if the prediction performance does not improve. These settings resulted in a moderate fit of the models to data, as shown later. We also attempted

211 settings that lead to underfitting and overfitting and compared them (see the "Algorithm assessment"
212 section). Lastly, there would be two choices for detecting the main effects of QTLs: using SHAP values
213 that contain interaction scores (i.e., φ_i) or using SHAP values from which interaction scores are
214 removed (i.e., φ_{ii}). In this study, the former score is referred to as "compound" scores, and the latter
215 is referred to as the "pure" scores for detecting QTL main effects. These two scores were compared as
216 described in the "Algorithm assessment" section.
217

218 **Comparing methods**

219 The SHAP-XGB method was compared with CIM, MIM, ICIM, and BayesC (Habier et al. 2011) using
220 simulated and real data. Note that BayesC and SHAP-XGB used only marker genotypes as covariates
221 and did not use the genotype probabilities of the loci between markers. For the CIM, MIM, and ICIM,
222 the intervals were set to 1 cM.

223 **Composite interval mapping (CIM)**

224 CIM was performed using the cim function of the R package qtl (ver. 1.60, Broman et al. 2003). The
225 expectation-maximization algorithm was used. The number of covariates was three, and the window
226 size was 10 cM. CIM was used to detect the main QTL effects. We assessed the influence of the number
227 of covariates and window size on the simulated and real data and found that the influence was
228 negligible (data not shown).

229 **Multiple interval mapping (MIM)**

230 MIM theory was first proposed by Kao et al. (1999). MIM assumes that the genotypic value is the sum
231 of multiple QTLs and QTL interaction effects. QTL genotypes are probabilistically represented using
232 neighboring marker genotypes and recombination frequencies; thus, the MIM model is a finite mixture
233 model. The QTLs and QTL interactions included in the model were searched in a stepwise manner.
234 MIM was conducted using the QTL cartographer (ver. 2.5_011, Wang et al. 2012). We followed the
235 algorithm proposed by Laurie et al. (2014). The algorithm consisted of multiple steps, including a
236 forward search of the main and interaction effects based on Bayesian information criteria, optimization

of QTL positions, and testing of QTL effects with a certain significance level (5%).

Inclusive composite interval mapping (ICIM)

Li et al. (2007) and Li et al. (2008) proposed the ICIM theory. ICIM consists of two steps: in the first step, markers and marker interactions significantly associated with phenotypes are selected with stepwise regression and one- or two-dimensional interval mapping is conducted in the second step by adjusting the phenotypes with the selected markers that are not related to the target intervals. The ICIM was performed using IciMapping (ver. 4.2.53, Meng et al. 2015). The *p*-values of the markers for entering models in stepwise regression (parameter PIN) were set to 0.001 for the main effects (option ICIM-ADD) and 0.0001 for mapping interaction effects (option ICIM-EPI). We attempted a higher PIN value for ICIM-EPI (0.01) in the simulated data; however, the influence was negligible (data not shown).

BayesC

We used BayesC as a representative Bayesian regression method because it circumvents a drawback relevant to degrees of freedom in parameter estimation (Habier et al. 2011). BayesC analysis was performed using the vigor function of the R package VIGoR (ver. 1.1.0, Onogi and Arakawa 2022). This package uses fast variational Bayesian algorithms to estimate the posterior distributions of Bayesian alphabets. The model included all markers and marker interactions (multiplications of marker genotypes) and estimated their coefficients simultaneously. The prior distribution of a coefficient was normal if the indicator of the marker (or marker combination) was 1 and 0 if the indicator was 0. The prior distributions of indicators were Bernoulli distributions with hyperparameters of 0.05 for main effects and 0.001 for interaction effects. Different prior normal distributions were assumed for main and interaction effects. Bootstrapping was applied to make the inferences about the indicators more robust. The model was fitted to bootstrap samples, and the posterior means of the indicators were averaged across the bootstrap samples. We used 1000 bootstrap samples in this study.

Simulations

263 The usefulness of SHAP-XGB was first investigated using simulations that mimicked biparental F_2
264 and RIL populations. The conditions of the simulations were as follows: The number of chromosomes
265 was 8, the length of each chromosome was 120 cM, the number of markers (SNPs) per chromosome
266 was 20, the number of QTLs was five, and the number of individuals was 200. The QTLs were assigned
267 so as to be one QTL per chromosome, and chromosomes harboring the QTLs were randomly selected.
268 Among the 10 combinations of QTLs, half were assumed to have interaction effects, and the
269 combinations with interaction effects were randomly selected. The main and interaction effects of the
270 QTLs were generated using the standard normal distribution. The broad-sense heritability was set at
271 0.8.

272 We simulated six scenarios using these conditions: (1) F_2 population with only additive effects
273 (QTL genotypes were coded as −1, 0, and 1). (2) RIL population with additive effects only. (3) F_2
274 population with only complete dominance effects (QTL genotypes were coded as 0, 1, and 1). (4) F_2
275 population with only overdominance effects (QTL genotypes were coded as 0, 1, and 0). (5) F_2
276 population with only additive effects and with epistatic variances increased by setting the variance of
277 interaction effects to 16. (6) F_2 population had only additive effects, but the number of QTLs with
278 nonzero additive effects was limited to two (i.e., three QTLs only had interaction effects without main
279 effects). (7) F_2 population with only additive effects, of which the size was increased to 400. (8) RIL
280 population with only additive effects, of which the size was increased to 400. When only additive
281 (dominance) effects were simulated, interaction effects were simulated as additive-by-additive
282 (dominance-by-dominance) effects by multiplying the corresponding QTL genotypes. A summary of
283 the simulation scenarios and realized proportions of variances due to the additive and interaction
284 effects are presented in Table 1. The QTLs and marker genotypes were generated using the R package
285 qtl (ver. 1.60). QTL effects and phenotypes were generated using house-developed R scripts. The
286 number of replications per scenario was 10, which was determined by considering the manual
287 operations for MIM and ICIM.

288 The accuracy of QTL detection was evaluated using receiver operating characteristic (ROC)

curves and the area under the curve (AUC). When drawing ROC curves, markers located within 20 cM of the QTLs were regarded as positive markers. For interaction effects, combinations of markers located within 20 cM of QTLs relevant to the interactions were regarded as positive combinations. ROC curves and AUC were calculated using the R package pROC ver. 1.18.0 (Robin et al. 2011). Differences in the AUC values between the methods were tested using the Wilcoxon signed-rank test (the significance level was 5% with Bonferroni correction). The global SHAP and global SHAP interaction scores were regarded as QTL signals for SHAP-XGB. The LOD scores were regarded as the signals for CIM and ICIM, respectively, and the bootstrap means of the marker indicators were regarded as the signals for BayesC. Because MIM implemented in QTL cartographers returns a list of detected QTLs and QTL interactions, ROC curves could not be drawn, and consequently, AUC could not be calculated (note that ROC curves require scores of all variables). Instead, the true and false positive rates were calculated.

Mapping dominance effects

Whereas the cim function of the qtl package, MIM by the QTL cartographer, and ICIM by QTL IciMapping test both the additive and dominance effects automatically, BayesC by vigor and SHAP-XGB need a specification which effect is targeted. Thus, for BayesC and SHAP-XGB, genotype codes were modified depending on the target effects. The genotypes were coded as [−1, 0, 1], [0, 1, 1], and [0, 1, 0] to test the additive, complete dominance, and overdominance effects, respectively.

Algorithm assessment

The performance of the compound and pure global SHAP scores in detecting QTL main effects was compared using simulation scenarios (1) (F_2 population with only additive effects), (5) (F_2 population with only additive effects and with increased epistatic variances), and (6) (F_2 population with only additive effects, but the number of QTLs that have non-zero additive effects was limited to two).

Two additional settings of XGBoost were compared to investigate the effects of the degree of fit

of the XGBoost models to the data on the QTL detection power. In the underfitting setting, the learning rate "eta" was set to 0.1 (default is 0.3) and the "max_depth," which specifies the maximum depth of trees, was set to 3 (the default is 6). The "early_stopping_rounds" was set to 3. In the overfitting setting, the hyperparameters were the default values and the number of rounds (boosting iterations) was set to 50 without early stopping. Simulation Scenarios 1 and 2 were used for comparison.

Real data

The real data were obtained from Onogi et al. (2016). Briefly, days to heading of rice were evaluated for 174 Koshihikari/Kasalath//Koshihikari backcross inbred lines (BILs) and their parental lines. The experiments were conducted in six experimental fields in Japan and Vietnam over three years, resulting in nine environments. The nine environments are summarized in Table 2, and details were provided in Table S1 in Onogi et al. (2016). The lines were genotyped for 162 biallelic markers.

Dependency plots

SHAP interaction values were calculated for each instance (line) because SHAP was originally proposed as a local importance measure. Thus, the interactions between QTLs (markers) can be visualized by plotting the SHAP interaction values of the marker combinations of interest for all lines. These plots are referred to as dependency plots. Dependency plots were constructed using the R package SHAPforxgBoost (ver. 0.1.1) with some modifications.

Results

There are two choices when applying SHAP values for mapping QTL main effects: using compound global SHAP scores that contain interaction scores or using pure global SHAP scores from which interaction scores are removed. We first compared these two types of values for mapping the QTL main effects in simulation Scenarios 1, 5, and 6. Scenario 1 simulated the F_2 populations with additive and additive-by-additive interactions. Scenarios 1 and 5 differed in the proportion of phenotypic

variance explained by epistatic variance (0.328 vs. 0.679 on average; Table 1), and Scenarios 1 and 6 differed in the number of QTLs that had main effects (5 vs. 2; Table 1). In Scenario 6, three QTLs only had interaction effects. The AUC values and ROC curves were comparable between the compound and pure scores (Figure S1). A slight increase in the detection power was observed for the compound scores in Scenario 5. In contrast, the false positive rates increased slightly for the compound scores in Scenario 6. This is reasonable because the three QTLs lacked main effects and only had interaction effects in Scenario 6. Thus, we concluded that the compound SHAP scores were comparable with or even better than the pure SHAP scores in QTL mapping as long as the QTLs that have non-zero main effects are involved in the interactions. Hereafter, we used compound scores to map the main QTL effects.

Next, we investigated the effect of the fitting degree of the XGBoost models on QTL mapping accuracy. We compared the three settings that led to underfitting, moderate fitting, and overfitting in simulation Scenarios 1 and 2. The SHAP values were either underestimated or overestimated when underfitting or overfitting was induced (Figure S2). Nevertheless, as the relative values between the markers did not vary significantly, the AUC values and ROC curves were hardly changed by the fitting status (Figure S3). We used a setting that induced a moderate fit.

In comparative analyses mapping main QTL effects, SHAP-XGB generally showed higher or comparable AUC values than CIM, ICIM, and BayesC (Figure 2). When compared with MIM, SHAP-XGB showed true positive rates comparable to MIM at the false positive rates that MIM showed (Figure 2). In comparative analyses mapping QTL interaction effects, SHAP-XGB showed significantly higher AUC values than ICIM and BayesC (Figure 3). When compared with MIM, SHAP-XGB showed higher true positive rates than MIM under false positive rates comparable to those of MIM (Figure 3), suggesting that SHAP-XGB can detect more QTL interactions than MIM under comparable false positive rates. Interactions between markers (QTLs) can be interpreted using dependency plots. The SHAP interaction values (local importance metrics) for a replication of Scenario 2 are shown in Figure 4. The effects of two QTLs, *QTL2* and *QTL3* tagged with *D3M19* and *D4M11* markers, respectively, were inverted depending on the genotype of *QTL4* tagged with *D6M1*. These

figures illustrate that dependency plots using local importance scores can facilitate the interpretation of interactions.

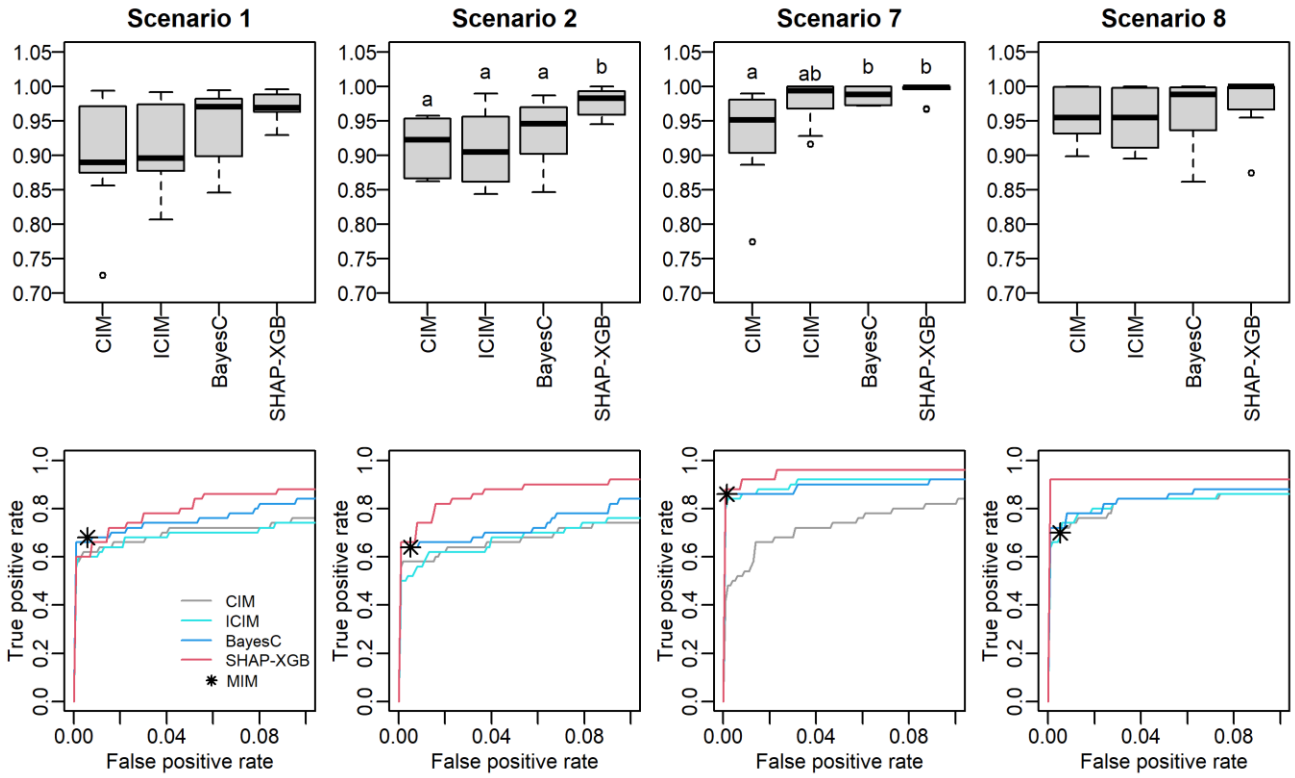

Figure 2 Area under the curve (AUC) values and receiver operation characteristics (ROC) curves in mapping main QTL effects. The top and bottom panels are the AUC values and ROC curves, respectively. The ROC curves are the mean curves of 10 replications. Scenarios 1 and 7 simulated F_2 populations, and Scenarios 2 and 8 simulated recombinant inbred line populations. The population sizes were 200 for Scenarios 1 and 2, and 400 for Scenarios 7 and 8. Different letters in the box plots denote significant differences (P <0.05). Because the results of MIM are the lists of detected QTLs, true and false positives are shown with the asterisk in the bottom plots. CIM: composite interval mapping, ICIM: inclusive CIM, SHAP-XGB: Shapley additive explanations-assisted XGBoost, MIM: multiple interval mapping.

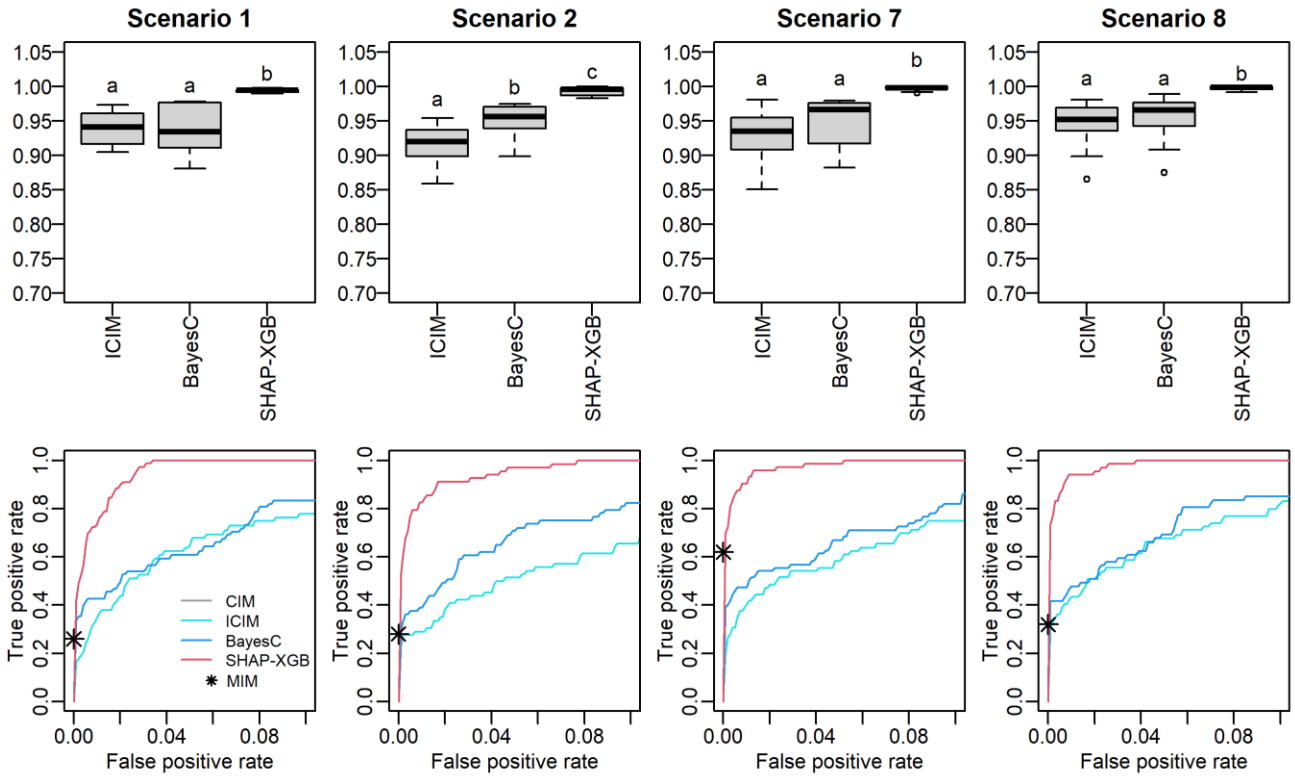

Figure 3 Area under the curve (AUC) values and receiver operation characteristics (ROC) curves in mapping QTL interaction effects. The top and bottom panels are the AUC values and ROC curves, respectively. The ROC curves are the mean curves of 10 replications. Scenarios 1 and 7 simulated F_2 populations and Scenarios 2 and 8 simulated recombinant inbred line populations. The population sizes were 200 for Scenarios 1 and 2, and 400 for Scenarios 7 and 8. Different letters in the box plots denote significant differences (P <0.05). Because the results of MIM are the lists of detected interactions, true and false positives are shown with the asterisk in the bottom plots. ICIM: inclusive composite interval mapping SHAP-XGB: Shapley additive explanations-assisted XGBoost, MIM: multiple interval mapping.

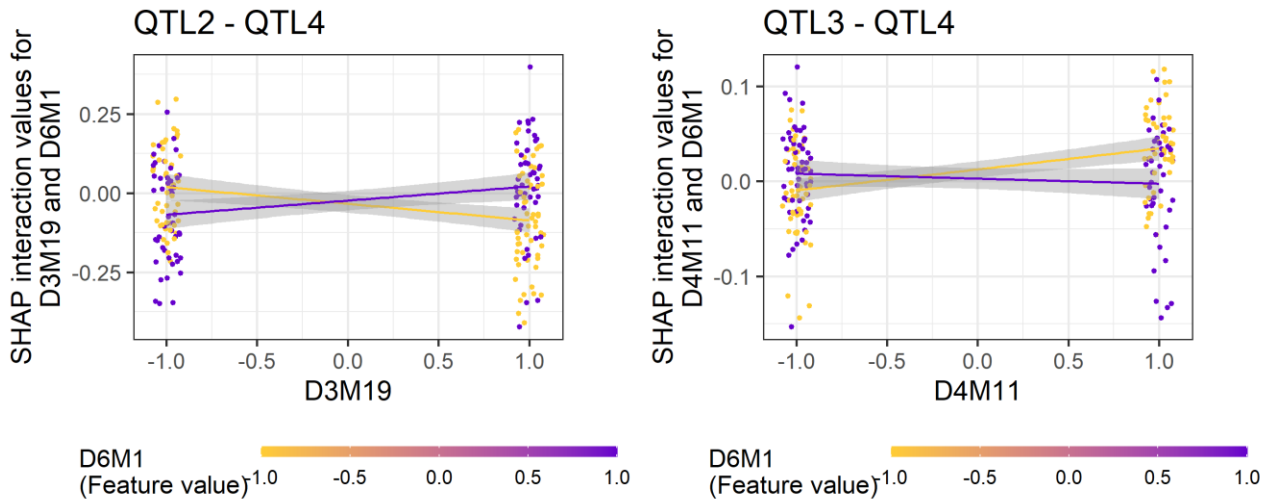

Figure 4 Dependencies between QTLs in a simulated dataset. The Shapley additive explanations (SHAP) interaction values of each line are shown as dots. The left panel shows the interaction between the 2nd and 4th QTLs, and the right panel shows that between the 3rd and 4th QTLs. *D3M19*, *D4M11*, and *D6M1* are the markers linked to the 2nd, 3rd, and 4th QTLs, respectively. Genotypes of *D6M1* are shown using different colors. Dots are scattered towards the x-axis. The regression lines were added for each genotype of *D6M1*. The shades denote the standard errors. The left panel shows that, when the genotype of *D6M1* is −1, SHAP interaction values (i.e., phenotypes) tend to decrease as the genotype of *D3M19* changes from −1 to 1, and when the genotype of *D6M1* is 1, SHAP interaction values tend to increase. The right panel shows inverted tendencies between *D4M11* and *D6M1*. The gray areas indicate the 95% confidence intervals of regression lines.

SHAP-XGB showed a performance comparable with that of CIM, MIM, ICIM, and BayesC for main effect mapping, and better than that of MIM, ICIM, and BayesC for interaction effect mapping in mapping dominance effects (Scenarios 3 and 4), as observed in mapping additive effects (Figure S4). In addition, SHAP-XGB showed comparable or only slightly decreased AUC values when additive effects were targeted than when dominance effects were targeted (Figure S5). These results are in contrast to those of BayesC, where misspecification of the target effects resulted in a more prominent decrease in accuracy. These results suggest that SHAP-XGB was insensitive to the effect type. This characteristic was also observed when dominance-by-dominance interactions were targeted. In other words, dominance-by-dominance effects can be detected even when additive-by-additive effects were targeted.

The XGBoost models explained 94.3% (± 1.9%) of the phenotypic variance with the setting of

413 moderate fitting in the real rice data analyses. SHAP-XGB and the compared methods showed similar
414 results in mapping the main QTL effects (Figure S5, Figure 5, and Table S1), and markers linked to
415 *Hd6* (chr. 3, Takahashi et al. 2001), *Hd1* (chr. 6, Yano et al. 1997), and *DTH8* (chr. 8, Wei et al. 2010)
416 showed higher signals for each method. The ICIM results were generally lenient when mapping
417 epistatic QTLs (Figure S6 and Figure 6), whereas the BayesC results were stringent (or conservative).
418 SHAP-XGB showed intermediate results between ICIM and BayesC, and could pinpoint interacting
419 combinations between known QTLs within reasonably narrow margins. The results of the MIM in the
420 mapping interactions were relatively stringent; nine interactions were detected in nine environments
421 (Table S1). In general, interactions were detected using SHAP-XGB. The global SHAP interaction
422 scores in each environment showed interesting trends across latitudes (Figure 7). Interactions between
423 *Hd1* and *Hd6*, *Hd1* and *DTH8*, and *Hd1* and *Hd2*/*OsPRR37* (Yano et al. 1997; Koo et al. 2013) showed
424 higher scores at higher latitudes (environments Tsukuba2007, Tsukuba2008E, Tsukuba2009,
425 Ishikawa2008, and Fukuoka2008), but lower scores at lower latitudes (environments Ishigaki2008,
426 HaNoi2008, and ThaiNguyn2008). In contrast, the interaction between *DTH8* and *Hd2* showed larger
427 scores at lower latitudes but lower scores at higher latitudes.
428

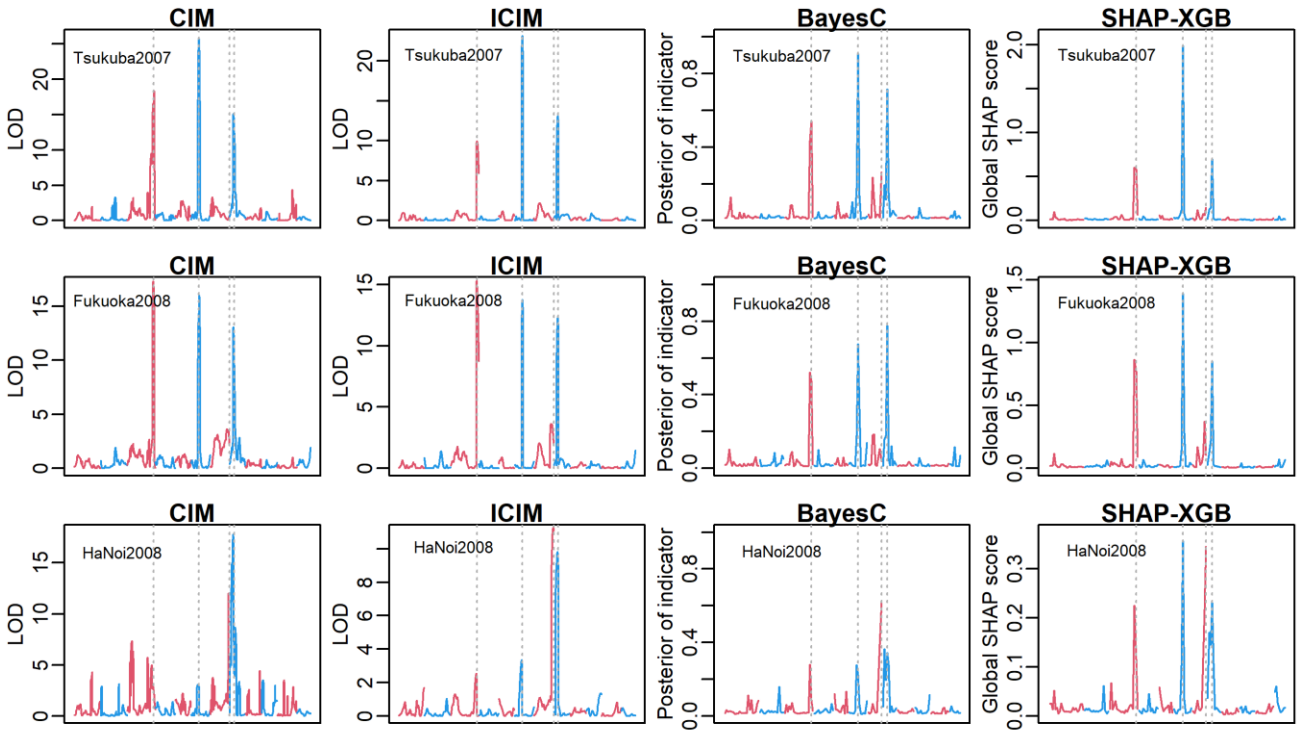

429

430 **Figure 5** Comparison of QTL mapping methods to detect main effects in the rice heading date data. The y-axis
431 denotes the QTL signals (CIM and ICIM, LOD score; BayesC, posterior indicator variable; SHAP-XGB, global
432 SHAP score). The x-axis denotes the chromosome positions. The neighboring chromosomes are distinguished
433 using different colors. The vertical bars indicate the four major QTLs (left to right, *Hd6*, *Hd1*, *Hd2*, and *DTH8*).
434 Note that, the x axes differed among methods because CIM and ICIM conducted interval mapping whereas
435 BayesC and SHAP-XGB used only marker genotypes as covariates. Three representative environments
436 (Tsukuba2007, Fukuoka2008, and HaNoi2008) are presented. The full results are shown in Figure S5. CIM:
437 composite interval mapping, ICIM: inclusive CIM, SHAP-XGB: Shapley additive explanations-assisted XGBoost.

438

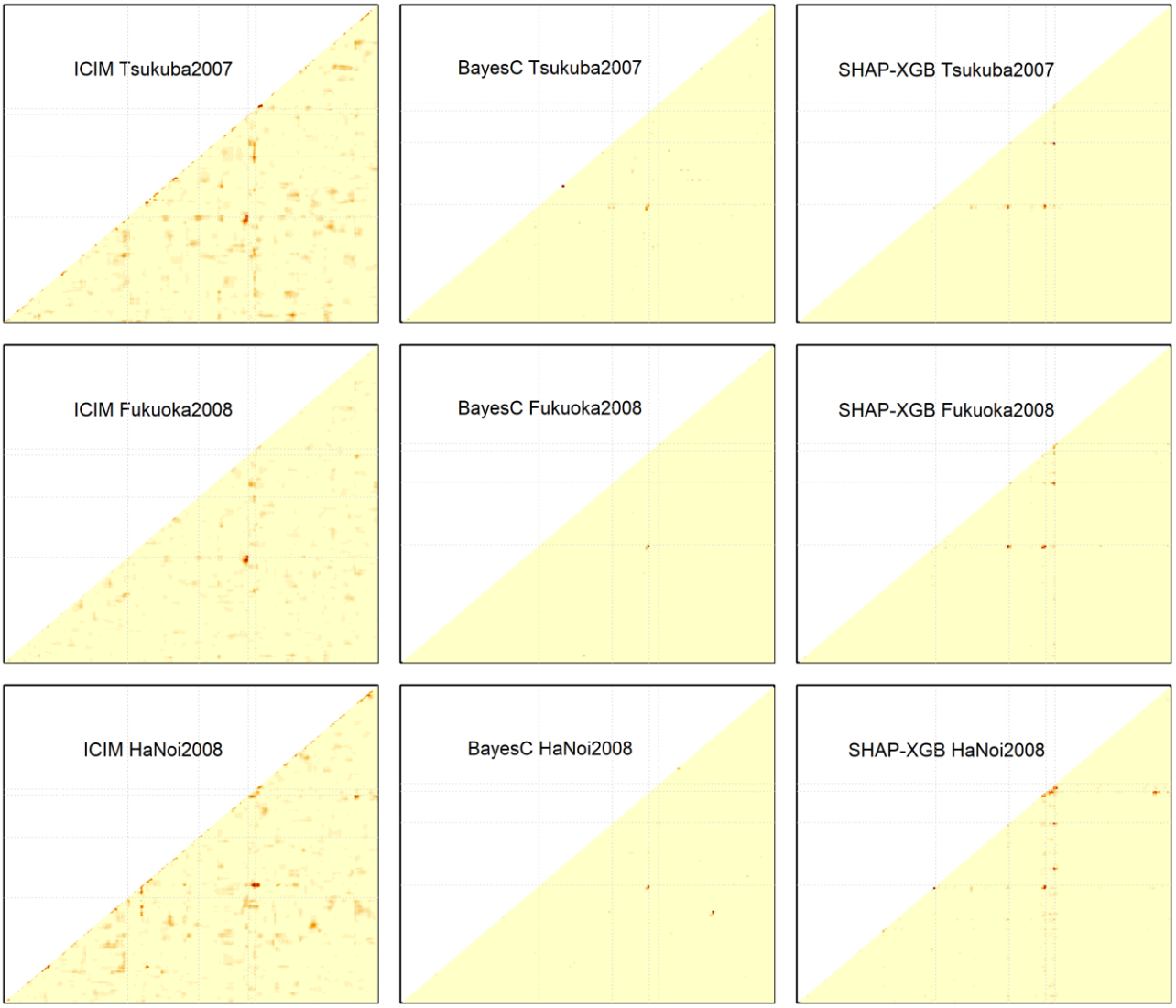

Figure 6 Comparison of QTL mapping methods to detect interaction effects in the rice heading date data. The y- and x-axes denote the relative positions of markers. The signal levels obtained with each QTL mapping method (ICIM, LOD score; BayesC, posterior indicator variable; SHAP-XGB, global SHAP interaction score) are shown using warm colors. The gray broken lines indicate the four major QTLs (left to right or bottom to top, *Hd6*, *Hd1*, *Hd2*, and *DTH8*). Note that positions of major QTLs in the x axes slightly differed among methods because CIM and ICIM used interval mapping whereas BayesC and SHAP-XGB used only marker genotypes as covariates. Three representative environments (Tsukuba2007, Fukuoka2008, and HaNoi2008) are presented. The full results are shown in Figure S6. ICIM: inclusive composite interval mapping, SHAP-XGB: Shapley additive explanations-assisted XGBoost.

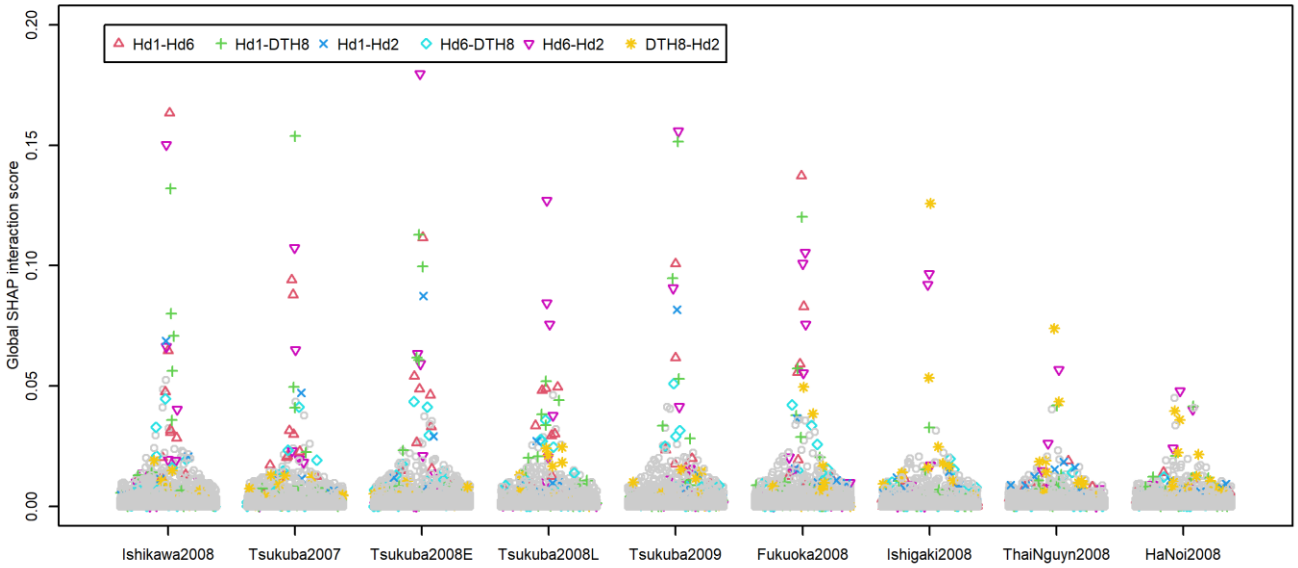

Figure 7 Summary of the global Shapley additive explanations (SHAP) interaction scores obtained in the rice heading date data. The y-axis denotes the global SHAP interaction scores, which are the averages of the absolute SHAP interaction values across all lines. The global SHAP interaction scores were horizontally jittered according to the densities of scores. The interaction values for the combinations of markers that were located within 20 cM from the known QTLs (*Hd6*, *Hd1*, *Hd2*, and *DTH8*) were regarded as the signals for the corresponding QTL interactions and highlighted using different colors and point shapes. The interactions between neighboring markers (< 20 cM apart) were removed for ease of visualization.

The interaction between *Hd1* and three QTLs (*DTH8*, *Hd6*, and *Hd2*) in Tsukuba2009 and the interaction between *DTH8* and *Hd2* in Ishigaki2008 were visualized using dependence plots (Figure 8). The Koshihikari allele (1) of *DTH8* and *Hd6* tended to shorten days to heading at Tsukuba2009 when the Koshihikari alleles were harbored at *Hd1*, whereas the Kasalath allele (−1) tended to prolong days to heading when the Kasalath alleles were harbored at *Hd1*. Contrasting tendencies were observed for the interactions between *Hd1* and *Hd2* in Tsukuba2009 and *Hd2* and *DTH8* in Ishigaki2008.

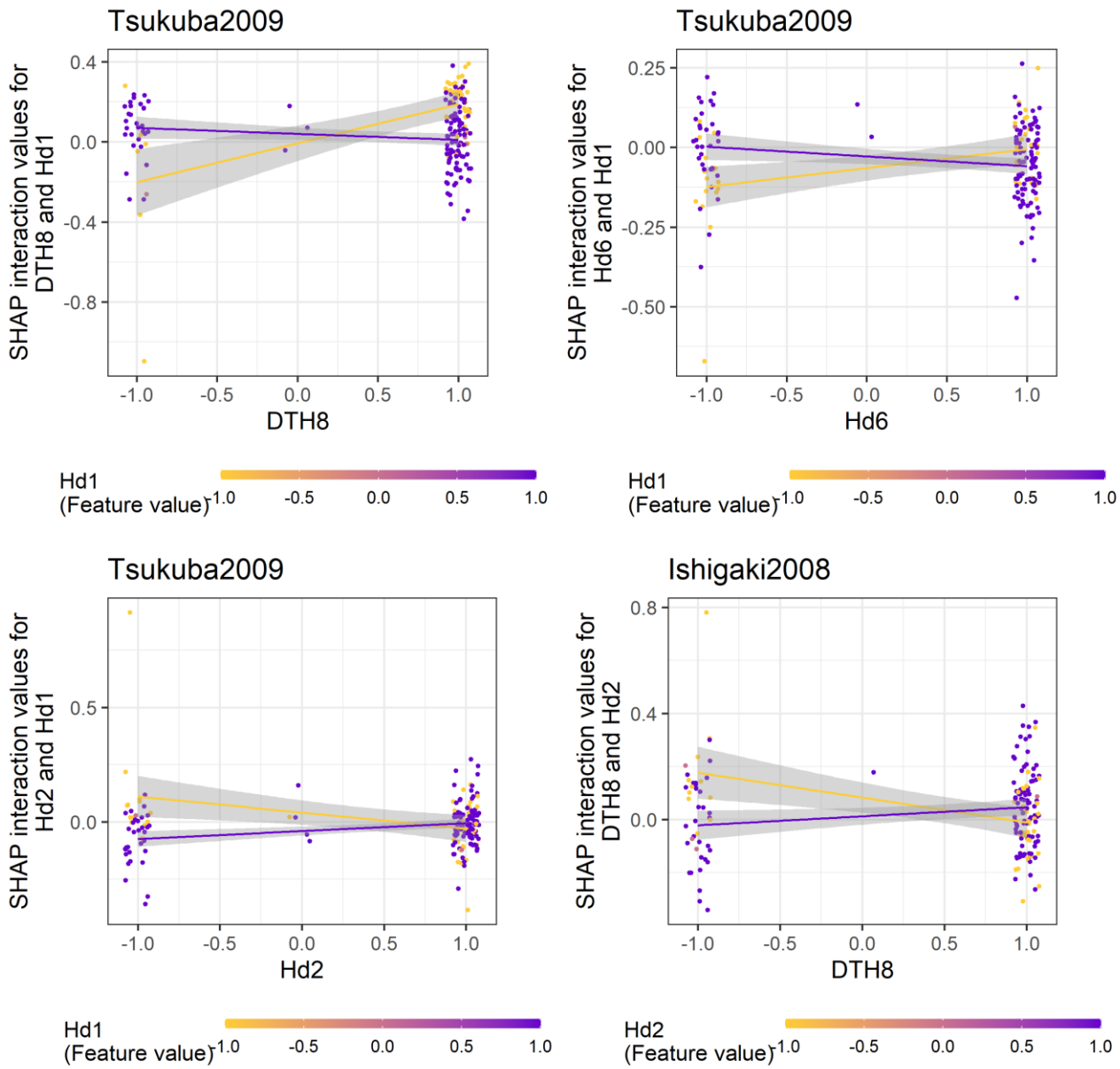

Figure 8 Dependencies between major QTLs shown with the Shapley additive explanations (SHAP) interaction values. The left top, right top, and left bottom panels show the dependency between *Hd1* and the three QTLs (*DTH8*, *Hd6*, and *Hd2*) at Tsukuba2009, respectively. The right bottom panel shows the dependency between *DTH8* and *Hd2* at Ishigaki2008. Each dot represents the SHAP interaction values for each line. Marker genotypes were regarded as the QTL genotypes. These markers were selected when the corresponding marker combinations showed the highest global SHAP interaction scores for the QTL interactions. For each panel and each QTL (marker), 1 and −1 indicate the Koshihikari and Kasalath alleles, respectively. The gray areas indicate the 95% confidence intervals of regression lines.

Discussion

We applied SHAP-assisted XGBoost (SHAP-XGB) to QTL mapping in biparental populations and compared it with conventional mapping methods in this study. SHAP-XGB generally showed comparable accuracy in finding QTL main effects with conventional methods and higher accuracy in finding epistatic QTL effects. The dependency plots enabled easy interpretation of the interactions. These results suggested that SHAP-XGB complements existing methods, particularly for identifying novel interactions between QTLs.

The simulation results revealed several properties of the SHAP-XGB. First, compound and pure global SHAP scores worked similarly to map the main effects of QTLs. While the compound scores showed slightly increased detection power when epistasis variances were larger, they also showed a slight increase in false positives when QTLs with interaction effects lacked the main effects. Thus, using compound scores may be advantageous as long as QTLs with non-zero main effects are involved in the interactions. Using compound scores may circumvent the reduction in pure scores due to LD, as described later. Second, the degree of fit (i.e., the extent to which the model fits the data) of the XGBoost models did not affect the QTL detection power. This is because the ROC curves and AUC values were calculated based on the relative rankings of markers that did not differ significantly depending on the fitting status. However, the result of over- or underfitting is the inflation or deflation of SHAP values, which in turn may make interpretations of SHAP values difficult. Thus, careful tuning of the fitting degree is recommended to improve interpretability. Finally, SHAP-XGB is robust to the misspecification of target effects, i.e., additive or dominance. That is, even when SHAP-XGB targets additive effects, it can map dominance effects or dominance-by-dominance interaction effects as accurately as the existing methods with correct target specifications. This property may be advantageous; however, it may be disadvantageous in some cases because the gene actions of the detected QTLs cannot be identified.

There are ways to measure feature importance for gradient boosting other than SHAP, including "gain" (the average increase of the objective function when the feature is added to trees) and "split

count" (the number of counts that trees split using the feature). Although these indices are provided by the R package of XGBoost, we did not adopt them because they do not hold the consistency property (Lundberg et al. 2018) and the package did not support them as importance of feature interactions. Nevertheless, considering that there are various indices to measure feature importance, such as local interpretable model-agnostic explanations (LIME) (Ribeiro et al. 2016) and the Shapley–Taylor interaction index (Sundararajan et al. 2020), it would still be worth investigating which indices are suitable for QTL mapping and whether the properties revealed here are applicable when SHAP is replaced with other indices. Such investigations are required to mitigate the negative effects of LD, as will be discussed later.

Although the simulated and real data analyses consistently suggest the usefulness of SHAP-XGB in QTL mapping, the marker genotypes have an undesirable property, i.e., LD between markers, for evaluating feature importance. Because XGBoost randomly samples markers to build a tree f, QTL effects are diluted with the markers linked to the QTLs, consequently decreasing the Shapley values of each linking marker. In fact, the global SHAP scores and SHAP interaction values in Figures 5 and 7 shrank to 0 (2.0 at most) considering that the units of the scores/values are the same as the phenotypic values (i.e., days). These decreased values were probably due to the correlated marker genotypes. The LD between the markers affected another aspect. In rice heading date analyses, interactions between neighboring markers were occasionally assigned large SHAP interaction values, resulting in a reduction in the main pure scores (these interactions were removed from Figure 7 for ease of visualization). However, such interactions are caused by LD between neighboring markers and thus should be interpreted as part of the main QTL effects. Although this decrease in pure main effects can be circumvented using compound scores for mapping, caution is required when interpreting pure scores. It has also been pointed out that approximations of Shapley values with SHAP become inaccurate when features are correlated (Aas et al. 2021) because the evaluations of the expectation in Eq. (2) assume independence between the features. Thus, taken together, LD would affect the detection power of SHAP-XGB. One solution is to replace SHAP with other indices that consider the

527 correlations among features (Aas et al. 2021).

528 Interactions between the major heading date QTLs weakened at lower latitudes (Figure 7 and
529 Table 2). These results were reasonable because *Hd6*, *Hd2*, and *DTH8* are involved in heading date
530 variation under long-day conditions (Hori et al. 2016; Wei et al. 2020). Interactions between *Hd1* and
531 three QTLs (*Hd6*, *Hd2*, and *DTH8*) are plausible under natural long-day conditions. For example,
532 interactions between functional *Hd6* alleles (e.g., Kasalath allele) and *Hd1* alleles (e.g., Nipponbare
533 allele) were reported under long-day conditions (Ogiso et al. 2010). Interactions between *Hd1* and *Hd2*
534 under long-day conditions (Lin et al. 2000), and interactions among *Hd1*, *Hd2*, *DTH8*, and *Ghd7* under
535 natural long-day conditions were also reported (Zhang et al. 2019). The interactions between *Hd2* and
536 *DTH8*, which is prominent in lower latitudes, are interesting but also plausible because interactions
537 between the functional/non-functional alleles of *Hd2* and *DTH8* alleles under natural short-day
538 conditions have been reported (Zhang et al. 2019). Thus, these results indicated the usefulness of
539 epistatic QTL mapping using SHAP-XGB for identifying novel interactions.

540 SHAP-XGB may be applicable to studies with denser DNA markers, e.g., GWAS; however, the
541 computational time and required memory size will increase. The increase in computational time
542 depends on the XGBoost fitting and SHAP value calculations. Fitting XGBoost to the rice real data (n
543 $= 176$ and $p = 162$) took 0.111 ± 0.055 seconds using a machine with Intel Corei7-13700k (3.40 GHz),
544 24 logical cores, and 128GB RAM, and calculation of SHAP and SHAP interaction scores took 0.007
545 ± 0.014 and 0.316 ± 0.144 seconds, respectively. We generated a feature matrix with $n = 1{,}760$ and p
546 $= 162{,}000$ from the standard normal distribution and fitted the SHAP-XGB to investigate the
547 scalability of SHAP-XGB. XGBoost took 51.34 seconds, and the calculation of SHAP took 430.89
548 seconds using the same machine, which is sufficiently practical. However, the calculation of the SHAP
549 interaction scores failed because of a memory allocation error, and this error could not be fixed until p
550 decreased to 2,000. SHAP interaction scores are calculated for all marker combinations in all samples
551 (i.e., an $n \times p \times p$ array is created), and the memory requirement may be a major bottleneck. Thus,
552 it may be necessary to prune markers using, for example, t-tests or sure independence screening (Fan

and Lv 2008). In GWAS, population stratification will be another issue. One solution would be to adjust the phenotypic values with population stratification before application.

The lack of thresholds for determining significant markers is a practical drawback for each application of SHAP-XGB (QTL mapping and GWAS). Permutation tests are one possible solution. Permutation tests are generally used to determine the thresholds for IM and CIM (e.g., Broman et al. 2003) and have been applied to detect gene-gene interactions based on the Shapley-based interaction score and neural networks (Cui et al. 2022). However, further investigation is required to determine whether these tests work as expected.

Data availability

Real data are shared at https://github.com/Onogi/HeadingDatePrediction. R scripts for SHAP-XGB are available at https://github.com/Onogi/SHAP-XGB.

Acknowledgements

The authors would like to thank Ryukoku University for providing financial support.

Funding

This study was supported by Ryukoku University.

Conflict of Interest

The authors declare no competing interests.

Author contributions

TI and AO collaborated in analyzing the data and drafting the manuscript. AO conceived the study.

References

Aas K, Jullum M, Løland A (2021) Explaining individual predictions when features are dependent: More accurate approximations to Shapley values. Artif Intell 298:103502. https://doi.org/10.1016/j.artint.2021.103502

Broman KW, Wu H, Sen S, Churchill GA (2003) R/qtl: QTL mapping in experimental crosses. Bioinformatics 19:889–890. https://doi.org/10.1093/bioinformatics/btg112

Chen T, Guestrin C (2016) Xgboost: A scalable tree boosting system. Proceedings of the 22nd ACM SIGKDD international conference on knowledge discovery and data mining 785–794. https://doi.org/10.1145/2939672.2939785

Crawford L, Zeng P, Mukherjee S, Zhou X (2017) Detecting epistasis with the marginal epistasis test in genetic mapping studies of quantitative traits. PLOS Genet 13:e1006869. https://doi.org/10.1371/journal.pgen.1006869

Cui T, El Mekkaoui K, Reinvall J, Havulinna AS, Marttinen P, Kaski S (2022) Gene-gene interaction detection with deep learning. Commun Biol 5:1238. https://doi.org/10.1038/s42003-022-04186-y

Falconer DS, Mackay TFC (1996). Introduction to quantitative genetics (fourth edition). Pearson Education Ltd, London.

Fan J, Lv J (2008) Sure independence screening for ultrahigh dimensional feature space. J R Stat Soc B 70:849–911. https://doi.org/10.1111/j.1467-9868.2008.00674.x

Fujimoto K, Kojadinovic I, Marichal J (2006) Axiomatic characterizations of probabilistic and cardinal-probabilistic interaction indices. Games Econ Behav 55:72–99. https://doi.org/10.1016/j.geb.2005.03.002

Habier D, Fernando RL, Kizilkaya K, Garrick DJ (2011) Extension of the Bayesian alphabet for genomic selection. BMC Bioinform 12:186. https://doi.org/10.1186/1471-2105-12-186

Hori K, Matsubara K, Yano M (2016) Genetic control of flowering time in rice: Integration of Mendelian genetics and genomics. Theor Appl Genet 129:2241–2252. https://doi.org/10.1007/s00122-016-2773-4

Jannink JL, Jansen R (2001) Mapping epistatic quantitative trait loci with one-dimensionalgenome

searches. Genetics 157:445–454. https://doi.org/10.1093/genetics/157.1.445

Jansen RC, Stam P (1994) High resolution of quantitative traits into multiple loci via interval mapping. Genetics 136:1447–1455. https://doi.org/10.1093/genetics/136.4.1447

Johnsen PV, Riemer-Sørensen S, DeWan AT, Cahill ME, Langaas M (2021) A new method for exploring gene-gene and gene-environment interactions in GWAS with tree ensemble methods and SHAP values. BMC Bioinform 22:230. https://doi.org/10.1186/s12859-021-04041-7

Kao CH, Zeng ZB, Teasdale RD (1999) Multiple interval mapping for quantitative trait loci. Genetics 152: 1203–1216. https://doi.org/10.1093/genetics/152.3.1203

Koo BH, Yoo SC, Park JW, Kwon CT, Lee BD, An G, Zhang Z, Li J, Li Z, Paek NC (2013) Natural variation in *OsPRR37* regulates heading date and contributes to rice cultivation at a wide range of latitudes. Mol Plant 6:1877–1888. https://doi.org/10.1093/mp/sst088

Lander ES, Botstein D (1989) Mapping Mendelian factors underlying quantitative traits using RFLP linkage maps. Genetics 121:185–199. https://doi.org/10.1093/genetics/121.1.185

Laurie C, Wang S, Carlini-Garcia LA, Zeng ZB (2014) Mapping epistatic quantitative trait loci. BMC Genet 15:112. https://doi.org/10.1186/s12863-014-0112-9

Li H, Ye G, Wang J (2007) A modified algorithm for the improvement of composite interval mapping. Genetics 175:361-374. https://doi.org/10.1534/genetics.106.066811

Li H, Ribaut JM, Li Z, Wang J (2008) Inclusive composite interval mapping (ICIM) for digenic epistasis of quantitative traits in biparental populations. Theor Appl Genet 116:243–260. https://doi.org/10.1007/s00122-007-0663-5

Li Z, Sillanpää MJ (2012) Estimation of quantitative trait locus effects with epistasis by variational Bayes algorithms. Genetics 190:231–249. https://doi.org/10.1534/genetics.111.134866

Lin HX, Yamamoto T, Sasaki T, Yano M (2000) Characterization and detection of epistatic interactions of 3 QTLs, *Hd1*, *Hd2*, and *Hd3*, controlling heading date in rice using nearly isogenic lines. Theor Appl Genet 101:1021–1028. https://doi.org/10.1007/s001220051576

Shapley LS (1953) A value for n-person games. Contributions to the Theory of Games 2.28, pp. 307–317

Lundberg SM, Lee S (2017) A unified approach to interpreting model predictions. Nips'17. Proceedings of the 31st international conference on neural information processing systems 4768–4777. Available from https://dl.acm.org/doi/10.5555/3295222.3295230

Lundberg SM, Erion GG, Lee S (2018) Consistent individualized feature attribution for tree ensembles. arXiv preprint arXiv:1802.03888. https://doi.org/10.48550/arXiv.1802.03888

Meng L, Li H, Zhang L, Wang J (2015) QTL IciMapping: Integrated software for genetic linkage map construction and quantitative trait locus mapping in biparental populations. Crop J 3:269–283. https://doi.org/10.1016/j.cj.2015.01.001

Ogiso E, Takahashi Y, Sasaki T, Yano M, Izawa T (2010) The role of casein kinase II in flowering time regulation has diversified during evolution. Plant Physiol 152:808–820. https://doi.org/10.1104/pp.109.148908

Onogi A, Watanabe M, Mochizuki T, Hayashi T, Nakagawa H, Hasegawa T, Iwata H (2016) Toward integration of genomic selection with crop modelling: The development of an integrated approach to predicting rice heading dates. Theor Appl Genet 129:805–817. https://doi.org/10.1007/s00122-016-2667-5

Onogi A, Arakawa A (2022) An R package VIGoR for joint estimation of multiple linear learners with variational Bayesian inference. Bioinformatics 38:3306–3309. https://doi.org/10.1093/bioinformatics/btac328

Ribeiro MT, Singh S, Guestrin C (2016) 'Why should i trust you?' Explaining the predictions of any classifier. Proceedings of the 22nd ACM SIGKDD international conference on knowledge discovery and data mining 1135–1144. https://doi.org/10.1145/2939672.2939778

Robin X, Turck N, Hainard A, Tiberti N, Lisacek F, Sanchez JC, Müller M (2011) pROC: an open-source package for R and S+ to analyze and compare ROC curves. BMC Bioinform 12:77. https://doi.org/10.1186/1471-2105-12-77

Sundararajan M, Dhamdhere K, Agarwal A (2020) The Shapley Taylor interaction index. Proceedings of the machine learning research 119:9259–9268. Available from https://proceedings.mlr.press/v119/sundararajan20a.html

Takahashi Y, Shomura A, Sasaki T, Yano M (2001) *Hd6*, a rice quantitative trait locus involved in

photoperiod sensitivity, encodes the alpha subunit of protein kinase CK2. Proc Natl Acad Sci U S A 98:7922–7927. https://doi.org/10.1073/pnas.111136798

Wang J, Joshi T, Valliyodan B, Shi H, Liang Y, Nguyen HT, Zhang J, Xu D (2015) A Bayesian model for detection of high-order interactions among genetic variants in genome-wide association studies. BMC Genom 16:1011. https://doi.org/10.1186/s12864-015-2217-6

Wang S, Basten CJ, Zeng ZB (2012) Windows QTL Cartographer 2.5. Department of Statistics, North Carolina State University, Raleigh, NC. (http://statgen.ncsu.edu/qtlcart/WQTLCart.htm)

Wei H, Wang X, Xu H, Wang L (2020) Molecular basis of heading date control in rice. aBIOTECH 1:219–232. https://doi.org/10.1007/s42994-020-00019-w

Wei X, Xu J, Guo H, Jiang L, Chen S, Yu C, Zhou Z, Hu P, Zhai H, Wan J (2010) *DTH8* suppresses flowering in rice, influencing plant height and yield potential simultaneously. Plant Physiol 153:1747–1758. https://doi.org/10.1104/pp.110.156943

Yano M, Harushima Y, Nagamura Y, Kurata N, Minobe Y, Sasaki T (1997) Identification of quantitative trait loci controlling heading date in rice using a high-density linkage map. Theor Appl Genet 95:1025–1032. https://doi.org/10.1007/s001220050658

Zeng ZB (1994) Precision mapping of quantitative trait loci. Genetics 136:1457–1468. https://doi.org/10.1093/genetics/136.4.1457

Zhang B, Liu H, Qi F, Zhang Z, Li Q, Han Z, Xing Y (2019) Genetic interactions among *Ghd7*, *Ghd8*, *OsPRR37* and *Hd1* contribute to large variation in heading date in rice. Rice (N Y) 12:48. https://doi.org/10.1186/s12284-019-0314-x

Zhang YM, Xu S (2005) A penalized maximum likelihood method for estimating epistatic effects of QTL. Heredity 95:96–104. https://doi.org/10.1038/sj.hdy.6800702

723 **Table 1** Simulation scenarios[1].

Scenario	Pop.	QTL effects[2]		Size	Proportion of variance[3]		Purpose	Results
		Main	Interaction		V_A	V_I		
1	F_2	A	A by A	200	0.476 ± 0.104	0.328 ± 0.112	Evaluation of QTL detection power	Figs. 2 and 3
							Comparison of pure and compound SHAP values	Fig. S1
							Comparison of XGB settings	Figs. S2 and S3
2	RILs	A	A by A	200	0.408 ± 0.175	0.385 ± 0.176	Evaluation of QTL detection power	Figs. 2, 3, and 4
							Comparison of XGB settings	Figs. S2 and S3
3	F_2	CD	CD by CD	200	0.417 ± 0.222	0.407 ± 0.212	Evaluation of QTL detection power (dominance)	Fig. S4
4	F_2	OD	OD by OD	200	0.462 ± 0.134	0.322 ± 0.130	Evaluation of QTL detection power (dominance)	Fig. S4
5	F_2	A	A by A	200	0.115 ± 0.037	0.679 ± 0.032	Comparison of pure and compound SHAP values	Fig. S1
6[4]	F_2	A	A by A	200	0.313 ± 0.178	0.476 ± 0.176	Comparison of pure and compound SHAP values	Fig. S1
7	F_2	A	A by A	400	0.630 ± 0.091	0.175 ± 0.087	Evaluation of QTL detection power in larger populations	Figs. 2 and 3
8	RILs	A	A by A	400	0.383 ± 0.218	0.423 ± 0.216	Evaluation of QTL detection power in larger populations	Figs. 2 and 3

724 [1]All populations were assumed to be derived from biparental crosses. SHAP: Shapley additive explanations, XGB: Xgboost.

725 [2]A: additive, CD: complete dominance, OD: overdominance.

726 [3]V_A: additive variance, V_I: epistasis variance.

727 [4]Scenario 6 simulated five QTLs, of which three only had interaction effects.

728 **Table 2** Nine environments in the rice heading date data[1].

Environment name	Location	Year	Transplanting date
Tsukuba2007	Tsukuba (N36°01'/E140°06')	2007	8 Jun.
Fukuoka2008	Fukuoka (N33°37' /E130°28')	2008	24 Jun.
HaNoi2008	HaNoi (N21°01' /E105°80')	2008	3 Jul.
Ishigaki2008	Ishigaki (N24°23' /E124°11')	2008	17 Jul.
Ishikawa2008	Ishikawa (N36°30' /E136°36')	2008	16 May
ThaiNguyn2008	ThaiNguyn (N21°35' /E105°49')	2008	15 Jul.
Tsukuba2008E	Tsukuba (N36°01' /E140°06')	2008 (Early sowing)	25 Apr.
Tsukuba2008L	Tsukuba (N36°01' /E140°06')	2008 (late sowing)	9 Jul.
Tsukuba2009	Tsukuba (N36°01' /E140°06')	2009	21 May

729 [1]Details of these environments are provided in Table S1 of Onogi et al. (2016).

730

Short Legends of Supporting Information

Figure S1: Comparison of area under the curve (AUC) values and receiver operating characteristics (ROC) curves between compound and pure global SHAP scores.

Figure S2: Comparison of the compound global SHAP scores obtained using the different XGBoost settings.

Figure S3: Comparison of the XGBoost settings in the simulated data sets.

Figure S4: Area under the curve (AUC) values and receiver operation characteristics (ROC) curves in mapping main (A) and interaction (B) effects when dominance effects were simulated (Scenarios 3 and 4).

Figure S5: Comparison of QTL mapping methods to detect main effects in the rice heading date data.

Figure S6: Comparison of QTL mapping methods to detect interaction effects in the rice heading date data.

Table S1: QTLs and QTL interactions detected with multiple interval mapping in the real rice data.

Abbreviations

AUC: Area under the curve

CIM: Composite interval mapping

ICIM: Inclusive composite interval mapping

IM: Interval mapping

LD: Linkage disequilibrium

MIM: Multiple interval mapping

QTL: Quantitative trait locus

ROC: Receiver operating characteristic

SHAP: Shapley additive explanations

SNP: Single nucleotide polymorphism

XGB: XGboost